

Integrated geophysical studies at ancient Itanos (Greece)

A. Vafidis^{a,*}, N. Economou^a, Y. Ganiatsos^a, M. Manakou^a, G. Poulioudis^a,
G. Surlas^a, E. Vrontaki^a, A. Sarris^b, M. Guy^b, Th. Kalpaxis^b

^a Applied Geophysics Laboratory, Mineral Resources Engineering, Technical University of Crete, Chania 73100, Greece

^b Laboratory of Geophysical-Satellite Remote Sensing and Archaeo-Environment, Institute of Mediterranean Studies, Foundation of Research and Technology (F.O.R.T.H.), Rethymno 74100, Greece

Received 18 June 2002; received in revised form 22 July 2004

Abstract

The results of an integrated geophysical survey at the archaeological site of Itanos (Crete) are presented and discussed. At Hellenistic Itanos, which is located near the seashore, the buried ruins are partially under the saline water table. The purpose of this geophysical survey was to map buried relics of buildings, streets and walls of ancient Itanos. In particular, the usefulness of combining conventional geophysical mapping techniques and high resolution imaging methods in delineating shallow targets of archaeological interest at such complex archaeological sites is studied.

Magnetic gradient, soil resistance and electromagnetic measurements were taken in grids covering an area of approximately 16,000 m². Processing of geophysical maps included filtering with the gradient and first derivative operators in the space domain and the upward continuation and Butterworth filters in the wavenumber domain. Emphasis is given to the mathematical description of the processing steps. The integration of the geophysical measurements revealed the existence of a well and three parallel walls verified by excavation. Ground probing radar and electrical tomography sections crossing the parallel walls showed the vertical extent of these features.

Ground penetrating radar time slices and 3D electrical tomography depth slices were used for the verification of specific anthropogenic anomalies, which were detected on the geophysical maps. A shallow seismic survey was carried out, in an effort to locate and map the ancient port. The combination of a wide spectrum of geophysical prospecting techniques was successful in delineating the buried relics, enhancing the information context regarding the Hellenistic settlement of Itanos, together with its port and necropolis. The geophysical survey at Itanos demonstrates that the integrated approach is appropriate for archaeological investigations at complex sites like Itanos.

© 2005 Elsevier Ltd. All rights reserved.

Keywords: Archaeological prospecting; Electrical tomography; Ground penetrating radar

1. Introduction

During the last decade, conventional high-resolution geophysical methods have been integrated with other techniques like ground penetrating radar, electrical

tomography and seismic refraction to maximize the information context of the subsurface relics [1,15,16,22–24,26,27]. Also, aerial photography and satellite remote sensing have been combined with ground-based geophysical data using geographic information systems [5,7,19].

An integrated geophysical survey was conducted at the archaeological site of Itanos located in Northeastern Crete, Greece (Fig. 1a). The geophysical mapping was carried out in selected grids (Fig. 1b) covering an area of

* Corresponding author. Tel.: +30 8210 37443; fax: +30 8210 64802.

E-mail address: vafidis@mred.tuc.gr (A. Vafidis).

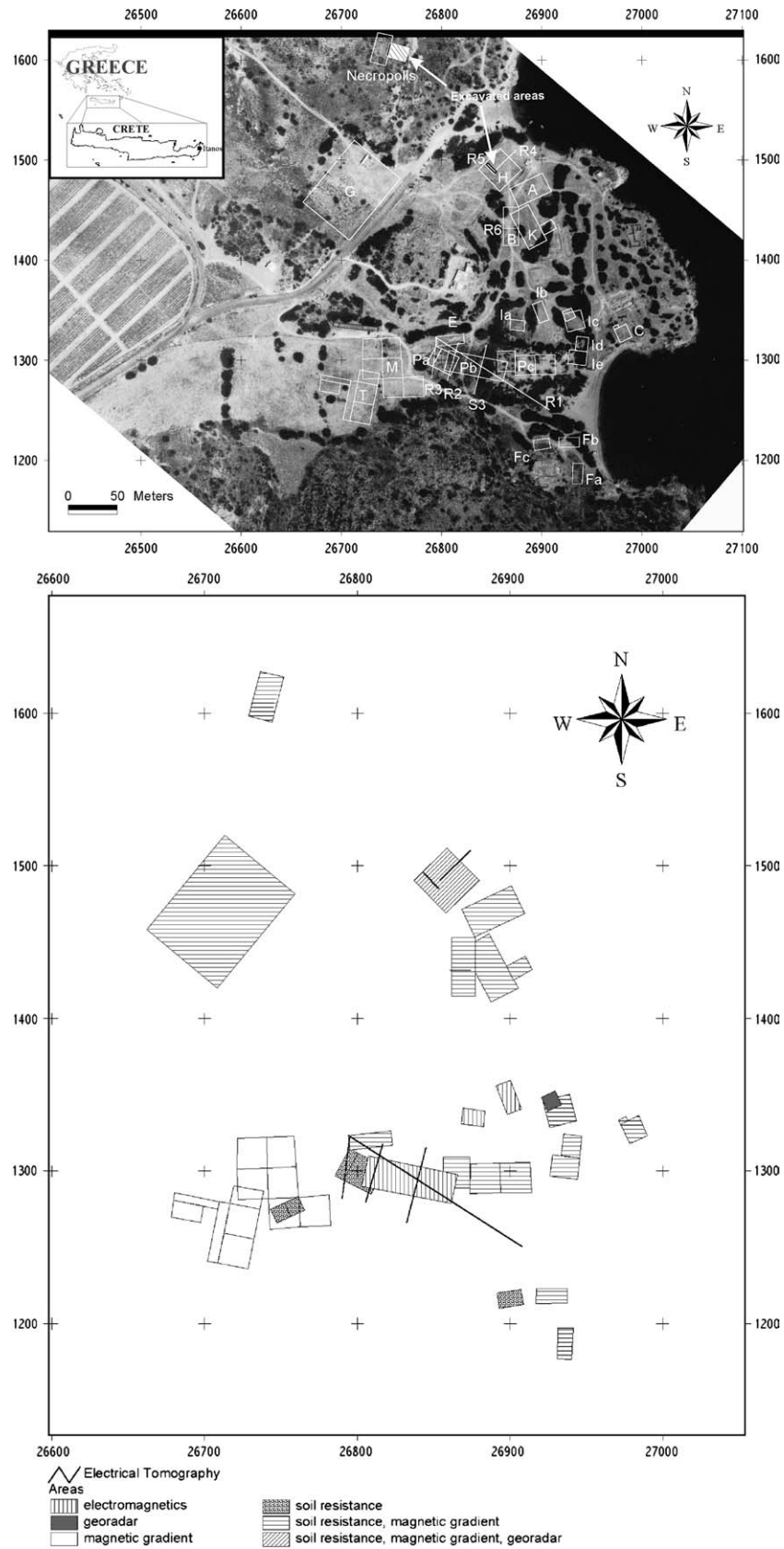


Fig. 1. (a) Air photograph of Itanos archaeological site showing the surveyed grids and lines (white) as well as the areas of excavation (indicated by white arrows). (b) The geophysical mapping techniques employed for each surveyed grid, as well as GPR and electrical tomography lines.

16,000 m². The grids were scanned with the magnetic method, the soil resistance method and the electromagnetic method. Additional measurements were taken with the electrical tomography technique, the ground penetrating radar and the seismic refraction. This paper presents the main results of the 5 year campaign of archeological prospecting surveying at the Hellenistic site of Itanos. The acquisition, processing and interpretation of the data are then presented and discussed in detail.

2. The archaeological site of Itanos

Itanos, an ancient coastal site in eastern Crete (Fig. 1a), is located 10 km north of Palaikastro, Lasithi prefecture, close to the unique Vai Palm Forest. The sea to the east, a mountain to the south and the provincial road to the west and north surround the archaeological site. There are two hills at (26800E, 1400N) and (27000E, 1400N) where the two acropolis of the ancient city are located. Most of the relics of the buildings of the ancient city have been located in the region between the acropolis.

According to a plan common in the Archaic Cretan cities, the houses and the market (agora) span the foothills of the two acropolis, while the religious monuments are located on the acropolis. A public building, probably a temple from the Hellenistic period, was found on the western acropolis. South of the two acropolis, the existence of a gulf suggests a potential location of the port. West of the gulf, we observe lowlands crossed by a modern paved road. On the higher hill south of the archaeological site, remnants of fortification walls are still present [10]. The inhabited region within the fortification does not exceed 400,000 m². The only known necropolis is extended to the north.

The name of the city, according to Stefanos from Byzantium, comes from Itanos, the son of Phoenix. Itanos according to Herodotus, the Greek historian, was one of the most important cities in eastern Crete in the middle of 7th century BC. It is among the first Cretan cities that cut coin (possibly at the beginning of the 4th century BC [8,10]).

The French archaeologist Demargne, started excavations in Itanos during the summer of 1899 [20]. In 1950, French archaeologists started a second and more systematic archaeological project. Itanos is marked mainly by three periods: Geometric, Roman and Late Christian, while the periods of original occupation and abandonment are not known. A new archaeological collaborative campaign between the French School at Athens and the Institute of Mediterranean Studies (Foundation of Research and Technology – FORTH) was initiated in 1993. Within the context of archaeological investigations, a geophysical prospecting expedition was also carried out.

3. Geophysical methods in archaeological investigations

In archaeological prospecting, magnetic measurements deal with anomalies of the geomagnetic field caused by contrasts of the rock magnetization or by variations of the magnetic properties of the soil. In archaeological investigations, various constructions, such as kilns, ovens or fireplaces, show increased remnant magnetization [13], thus producing pronounced magnetic anomalies. Also, remnant magnetization is detected in burned soils, rich in organic material and in man-made structures like filled pits, ditches filled with soil and excrement.

At Itanos, the vertical gradient of the Earth's magnetic field was measured [4] using the Geoscan Fluxgate gradiometer FM18 and the Geometrics Proton Precession Magnetometer G-856A. Geological magnetic trends and diurnal variations of the magnetic field did not affect magnetic gradient data.

The resistivity method was also employed, since it was expected that the ancient relics could produce remarkable resistivity contrast with respect to the surrounding soil [3,18]. Although the rocks show a large range of resistivity values, in archaeological investigations it is accepted that the building materials have in general larger resistivities than those of sandy soils and shales [28]. At Itanos, we utilized the Geoscan RM15 twin probe array consisting of two remote electrodes (M, A) and two mobile ones (N, B), with electrode separation of 1 m to 2 m (effective depth of 1–2.5 m; [19,25]).

The electromagnetic (EM) method determines the electric and magnetic properties of the rocks from the observations of induced EM fields [9]. The EM method, being used in archaeological prospecting since the 1960s, suffers from limitations in the resolution as well as ambiguities in the interpretation [21]. The electromagnetic induction instrument Geonics EM-31, used at Itanos, measures the in-phase and quadrature components of the secondary electromagnetic field. The quadrature component depends on soil conductivity. Thus, from the quadrature component measurements, the soil conductivity is estimated [12].

Electrical tomography surveys can be used to delineate areas with complex subsurface geology where conventional resistivity sounding or profiling is inadequate [14]. At Itanos, the Sting R1/Swift system was used to collect data along specific traverses, which were contoured in the form of a pseudosection, giving an approximate picture of the subsurface resistivity. Accurate depth determination and interpretation was achieved through inversion of the measured apparent resistivity.

Ground penetrating radar (GPR) employs radio waves, typically in the 1–1000 MHz frequency range, to provide information about the stratigraphy of

a site [6]. The most widely used mode of GPR surveying is common-offset, single fold reflection profiling. In such a reflection survey, a system with fixed antenna geometry is transported along a survey line. Radio energy transmitted into the subsurface, is reflected by the structural boundaries, and is returned to the receiver. The subsurface can be viewed and interpreted as the data are collected, making this technique very appealing and popular.

Shallow reflection and refraction seismic studies were carried out at Itanos in order to map the top of the basement (hard rock) as well as the thickness of the overburden which consists of recently deposited sediments. Seismic refraction is especially suited for the investigation of boundaries in shallow depth [22]. The total length of a seismic array and the geophone interval determine the penetration depth of a seismic refraction survey.

4. Magnetic, soil resistance and electromagnetic survey

The grids covering an area of 16,000 m² (Fig. 1b) were scanned with magnetic (vertical magnetic gradient), soil resistance and electromagnetic methods in order to map the city plan of Itanos including its harbor. During data acquisition, station spacing was 1 m and measurements were taken along common lines of adjacent grids. Measurements on adjacent grids may show deviations due to differences resulting from the

calibration of the magnetic instrument or the position of remote electrodes in soil resistance techniques. Edge matching of adjacent grids is based on the calculation of the mean value of measurements along the common lines. For grids with common lines in one to four sides of the grid, a trial and error method, based on the average value of the whole grid, is applied in order to determine the correction factor for each grid [17].

For the preparation of the geophysical maps kriging is performed on the data. Kriging involves the construction of a smooth surface from the data with a minimum curvature interpolation method. After obtaining an acceptable minimum curvature surface, the cell is subdivided and the same procedure is repeated until the cell size of the minimum curvature surface is equal to the grid spacing.

The geophysical maps (Figs. 2, 3) indicate a number of anthropogenic features. The magnetic gradient map (Fig. 2a) shows a series of parallel linear anomalies H1, H2, H3 and H4 aligned in the SW–NE direction. Most of the above anomalies were also registered in the soil resistance measurements (Fig. 2b). In addition, the soil resistance map indicates another smaller linear anomaly H8 further to the south, together with a circular anomaly H7 to the northeast. It is probable that the above anomalies represent the remains of a structural anomaly, which is limited by a perpendicular anomaly H6 to the north.

Grid K (Figs. 1a and 2a,b) also shows a few prominent anomalies including K1, K2 and K5. A well

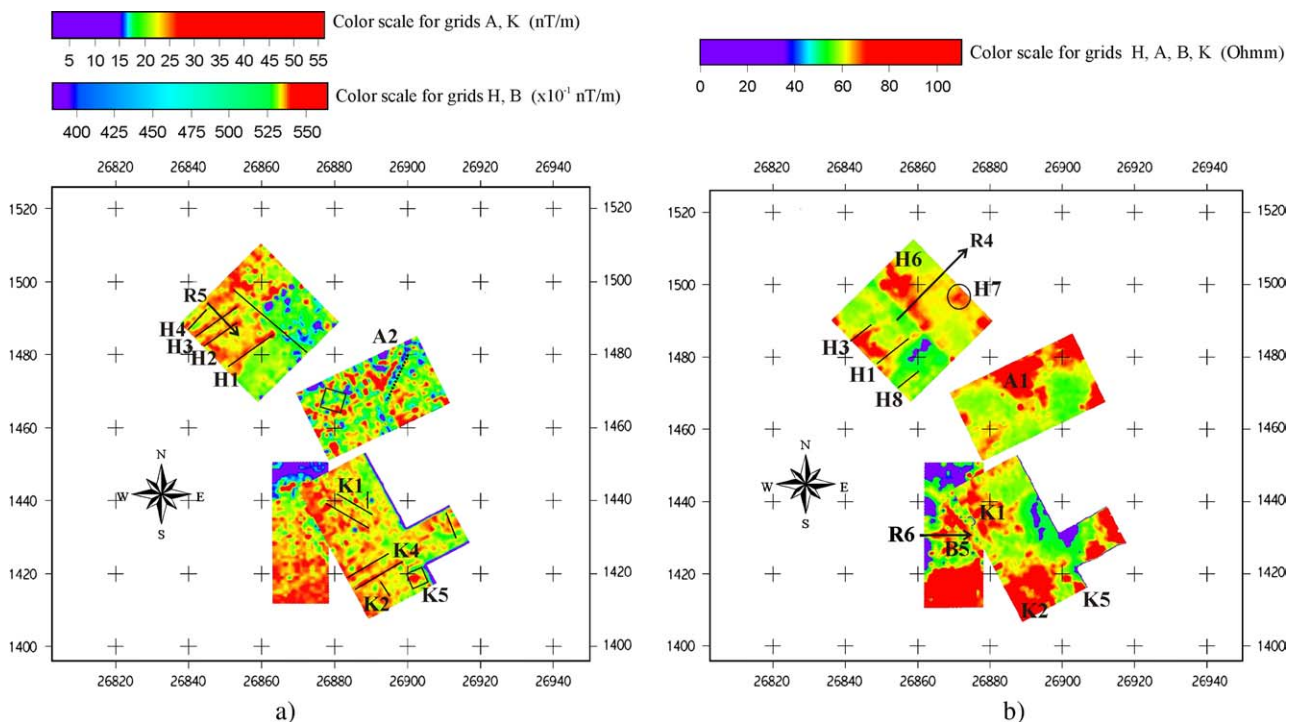


Fig. 2. Geophysical maps for grids H, A, B and K: (a) magnetic gradient and (b) soil resistance.

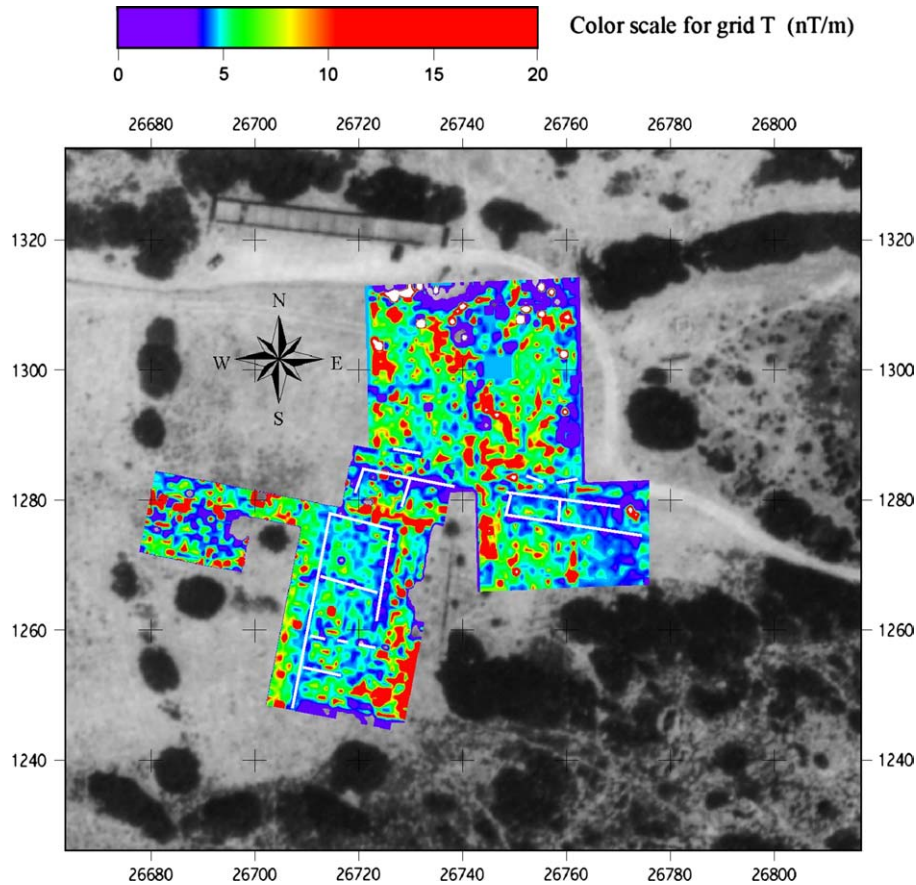


Fig. 3. Magnetic gradient map of grid M. The background picture is the air photograph.

constructed with ceramic bricks (Fig. 12) and layers of burned soils, which were found by excavation, caused the anomaly K5. On the magnetic gradient map (Fig. 2a) an elongated anomaly K4 is also observed probably related to a corridor found further to the east. The extension of K4 is observed at the lower part of the magnetic gradient map (grid B, Fig. 2a). Successive rectangular and linear high resistivity anomalies B5 are attributed to remnants of buildings and/or streets. In grid A (Fig. 1a), the soil resistance map (Fig. 2b) shows the high resistance anomaly A1 on the central part. An elongated anomaly A2 is present on the magnetic gradient map (grid A, Fig. 2a). In grids M and T, the magnetic gradient map images a portion of the city plan (Fig. 3).

4.1. Processing of geophysical data

Generally, most geophysical data sets do require processing but few of the available packages give the background of what the processing entails. Thus, most papers of geophysical surveys do not describe the mathematics of the processing. In this paper an explicit effort is made to present the processing methods. In the

processing software Transform V3.4, users can develop their own algorithms.

The following differential operators were applied to the data from geophysical mapping at Itanos [2].

- The gradient operator $\sqrt{\{(\partial_x Z)^2 + (\partial_y Z)^2\}}$ where Z denotes the measurements and ∂_x , ∂_y the partial differential operators with respect to x and y , generates a grid of steepest slopes.
- The first derivative along the x -axis is described by the operator $L_x = k_x i$, where $i = (-1)^{0.5}$ and k_x denotes wavenumber in the x direction.
- The Laplacian operator provides a measure of discharge (negative values) or recharge (positive values) on a surface. It is described by the operator $L_2 = (ri)^2$ where r is the radial wavenumber $r = \sqrt{(k_x^2 + k_y^2)}$ and k_x , k_y denote wavenumbers in the x and y directions.

Upward continuation of potential fields acts as a smoothing filter. The field at a height h above the ground (here $h = 3\text{--}8$ m) is considered as the regional field. In order to apply upward continuation, the data were transformed in the wavenumber domain using the

two-dimensional (2D) Fast Fourier transform. Before transforming the data, the map was padded with zeros so that its dimensions be a power of two. Tapering was also applied on the data with a 2D Hanning filter [11] to reduce wraparound errors. Upward continuation in wavenumber domain was performed by simply multiplying the transformed map with the operator: $L = e^{-hr}$. The regional field resulted by transforming the data back to the space domain. Apart from upward and downward continuation in the wavenumber domain, other operators like the directional derivative L_x and the Laplacian L_2 were also applied in the wavenumber domain. Additionally, a highpass Butterworth filter was used to enhance the local field. Its operator in the wavenumber domain is described by

$$L_b(r) = 1 - \frac{1}{1 + (r/r_c)^n} \quad (1)$$

where r_c is the cutoff radial wavenumber, and n is the order of the Butterworth filter (here $n=8$) which controls its slope. If Gibbs phenomena are present, the order of the filter must be reduced. The cutoff wavenumber can take values from 0 to $r_{nyquist}$ ($=0.5/\text{m}$ for grid spacing 1 m). The algorithms mentioned above were applied to all data sets of geophysical mapping, but in this paper selected geophysical maps are presented.

The application of a highpass Butterworth ($r_c = 0.2/\text{m}$) filter in the soil resistance data of grid H (Fig. 4a) enhanced the anomalies H1, H6 and H8. Parallel elongated anomalies H1, H2, H3, H4 and H5 were emphasized in the highpass filtered data of magnetic gradient (Butterworth, $r_c = 0.2/\text{m}$, Fig. 4b). Features H8 and H6 are also present in the quadrature data filtered with the gradient operator (Fig. 4c). The above advocate the existence of more than one closed structure in grid H, which probably belong to the coastal facilities of the settlement.

Most of the mentioned anomalies are shown on the magnetic map (Fig. 4d) which was generated by calculating the upward continued field at $h = 5$ m and subtracting it from the measured magnetic field. Excavations that followed brought to light parallel walls at distances 4.5 m, 6–7 m and 9–9.5 m from the NW edge of the grid and at depths of 0.7 m, 0.4 m and 0.25 m respectively (Figs. 9a and 11). More specifically, the walls at distances 4.5 m and 9–9.5 m are related to the observed anomalies H3 and H2, respectively.

In grid K, the quadrature map suggested an elongated anomaly K6 attributed to the sewage system (Fig. 5a). The quadrature map, filtered by a directional derivative operator (Fig. 5b), emphasized the elongated anomaly K4. The soil resistance gradient map (Fig. 5d) and the high pass filtered magnetic gradient map ($r_c = 0.125/\text{m}$) (Fig. 5c) indicated the same anomaly K5

which was attributed to the existence of a well constructed by ceramic bricks and stones (Fig. 12).

In conclusion, processing of the geophysical data was of extreme help in suggesting several potential targets. In grids K, A and B, a small portion of the city plan is imaged. A small portion of the city plan is also imaged in grids M and T. Grid H, apart from the three excavated walls (Fig. 11), encounters a wealth of anthropogenic anomalies. The interpretation of the geophysical anomalies is expected to modify based on the results of future excavations.

5. Electrical tomography

2D and 3D electrical tomography measurements were collected at Itanos using the Wenner, the pole–pole or the dipole–dipole arrays with electrode spacing ranging from 0.5 m to 5 m. The data were contoured in the form of a pseudosection. To obtain a more accurate picture of the subsurface it is necessary to invert the apparent resistivity data. The inversion method was based on a smoothness-constrained least squares method (Gauss–Newton method [14]).

Fig. 6a shows the resistivity section for line R5 next to the excavated trench (grid H, Fig. 9a). This resistivity section exhibits a series of high resistivity anomalies. It helps in delineating the elongated anomalies H3 and H2 present on the soil resistance and magnetic gradient maps (Fig. 2). The high resistivity anomaly W1 is attributed to the wall revealed at horizontal distance 4.5 m in the excavated trench (Figs. 9a and 11). Similarly, the anomalies W2 and W3 are attributed to the walls at 6–7 m and 9–9.5 m (Figs. 9a and 11).

Line R4 runs in a direction perpendicular to the excavated trench. The series of high resistivity anomalies on the resistivity section (Fig. 6b) are located at depths greater than 1.5 m except the one at horizontal distance 17–18 m, which is attributed to the extension of the elongated anomaly H6 present on the soil resistance map (Fig. 2b).

Fig. 6c shows the resistivity section for line R6 on grid B (Fig. 1a). The dipole–dipole array was used with electrode spacing of 1 m. The location of the first electrode was 1 m outside the grid. High resistivity zones are observed at 0.5–2 m, 5–6 m, 7–8 m, and 9–10 m whose depth is less than 1 m. This resistivity section which crosses the high resistivity anomaly B5 on the soil resistance map (Fig. 2b) indicates that this anomaly is caused by shallow high resistivity structures (such as wall remnants).

Grid P, consisting of subgrids P_a, P_b and P_c (Fig. 1), was scanned with the magnetic gradient, soil resistance and electromagnetic methods. Electrical tomography measurements were carried out on grid P with electrode spacing ranging from 1.5–5 m using the dipole–dipole

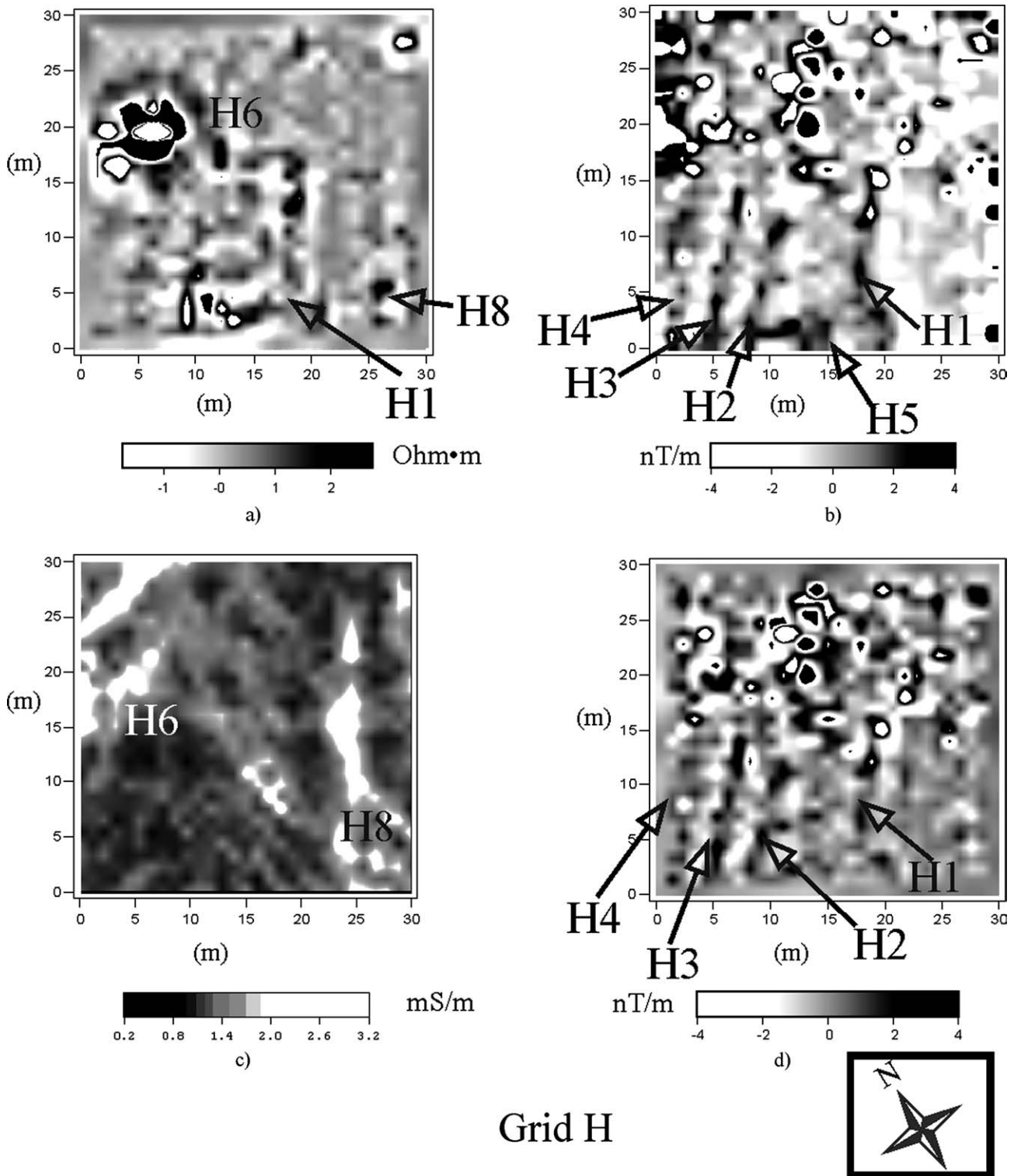


Fig. 4. Geophysical maps for grid H (a) high-pass filtered (Butterworth) soil resistance map, (b) high-pass filtered (Butterworth) magnetic gradient map, (c) quadrature map filtered with a gradient operator and (d) residual magnetic map which is generated by upward continuation of the original magnetic gradient data.

array. The resistivity sections for lines R2 and R3 (Fig. 8b,c) exhibit high resistivity anomalies P1 and P2 located at depths less than 2 m and present on the soil resistance map (Fig. 7).

A three-dimensional image constructed from electrical tomography data along three parallel lines (line interval 0.5 m and probe spacing 0.5 m) at the Necropolis, near the excavated area (Figs. 1a and 8d),

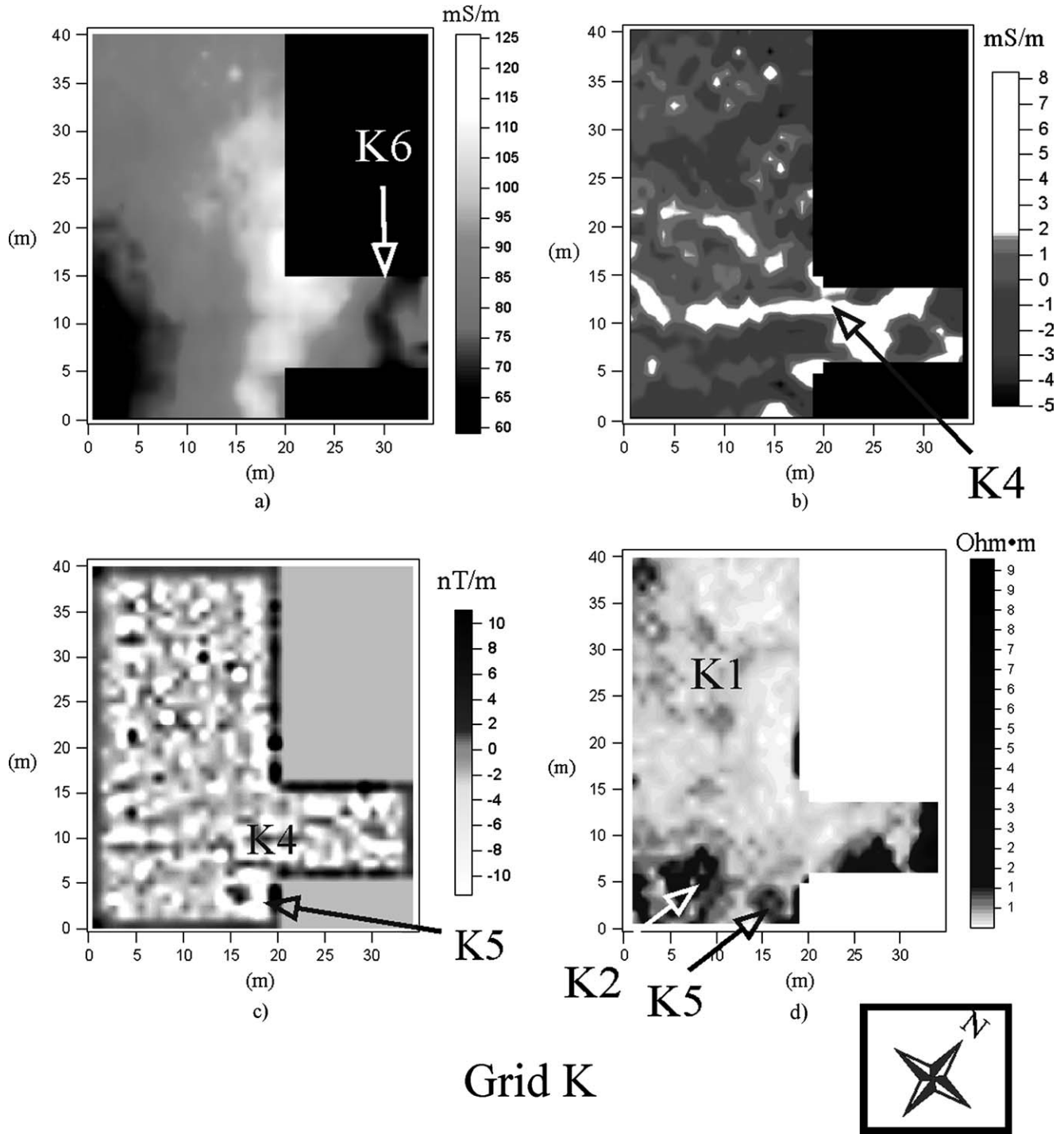


Fig. 5. Geophysical maps for grid K: (a) quadrature map, (b) quadrature y-derivative map, (c) high-pass filtered (Butterworth) magnetic gradient map and (d) soil resistance gradient map.

shows a shallow linear anomaly EB. The high resistivity anomaly EA (Fig. 8d) is attributed to a wall, partially revealed in the excavated area.

6. Ground penetrating radar

The 225 MHz and 450 MHz antennas of a PULSE EKKO 1000 ground penetrating radar system were used

with line spacing 1 m (station spacing 0.1 m) and 0.5 m (station spacing 0.05 m), respectively. On grid H, 50 NW-SE 30 m long lines were surveyed with the 225 MHz antennas (Fig. 9a). A portion of the same grid (nine 12-m long lines) was also scanned with the 450 MHz antennas (Fig. 9a). The radargrams along the line HR (Fig. 9a) show diffraction patterns at $x=4.4$ m and 6 m on a common depth point (CDP) gather from grid

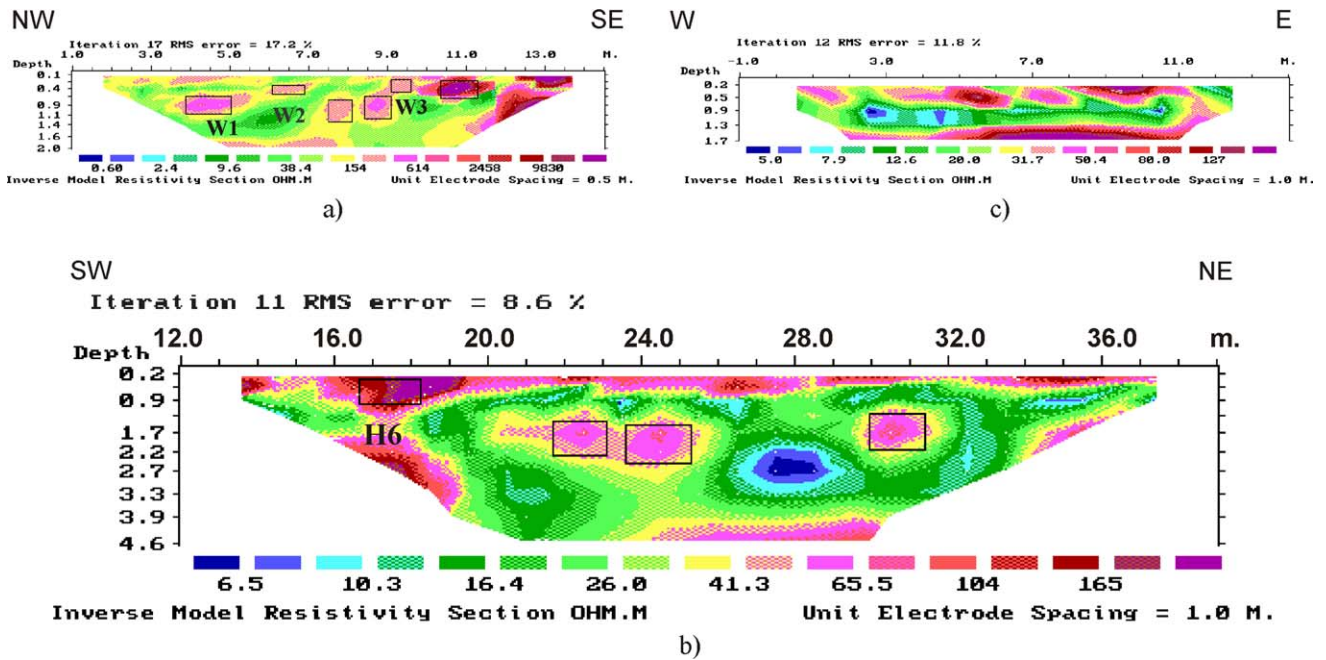


Fig. 6. Electrical tomography sections for lines (a) R5, (b) R4 and (c) R6 on grids H and B.

H (Fig. 9c). These diffractions were better resolved with the 450 MHz antennas (Fig. 9d) and are attributed to walls buried at a depth of 0.15 m (3 ns).

Time slices at 2–3 ns and 4–5 ns were obtained by interpolating the 225 MHz antennas raw data with the

Surfer 6 software package (Fig. 9e,f). These time slices exhibit features (black) which correspond to the anomalies on soil resistance, magnetic gradient and conductivity maps discussed earlier. In particular, the anomaly H6 is divided in two parallel NW-SE anomalies

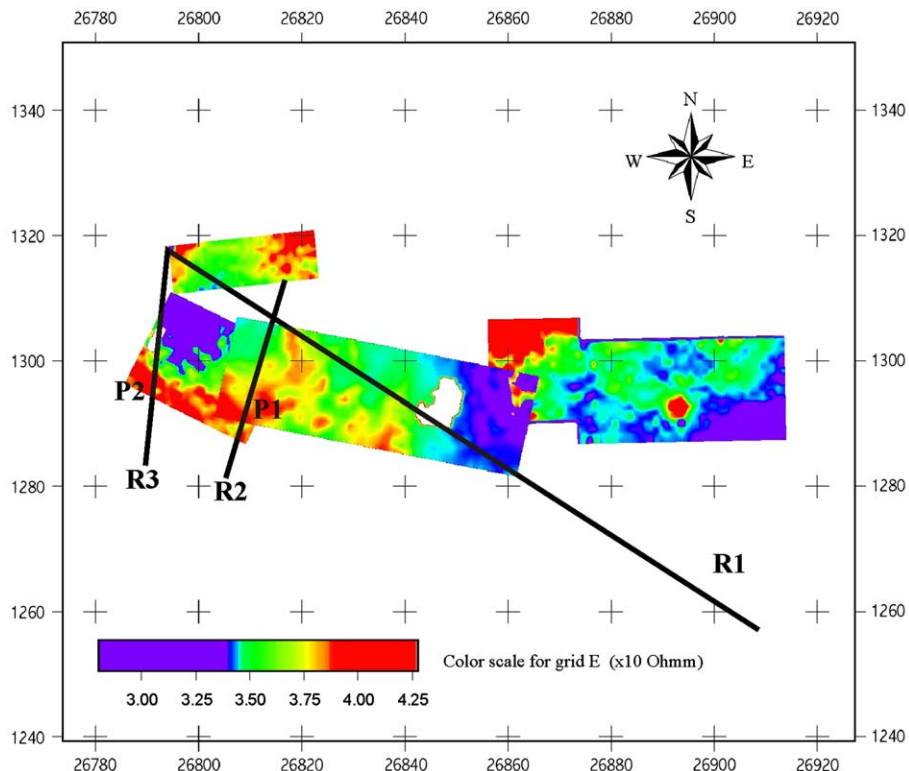


Fig. 7. Geophysical survey at the port. Soil resistance map for grids P and E and electrical tomography lines R1, R2, R3.

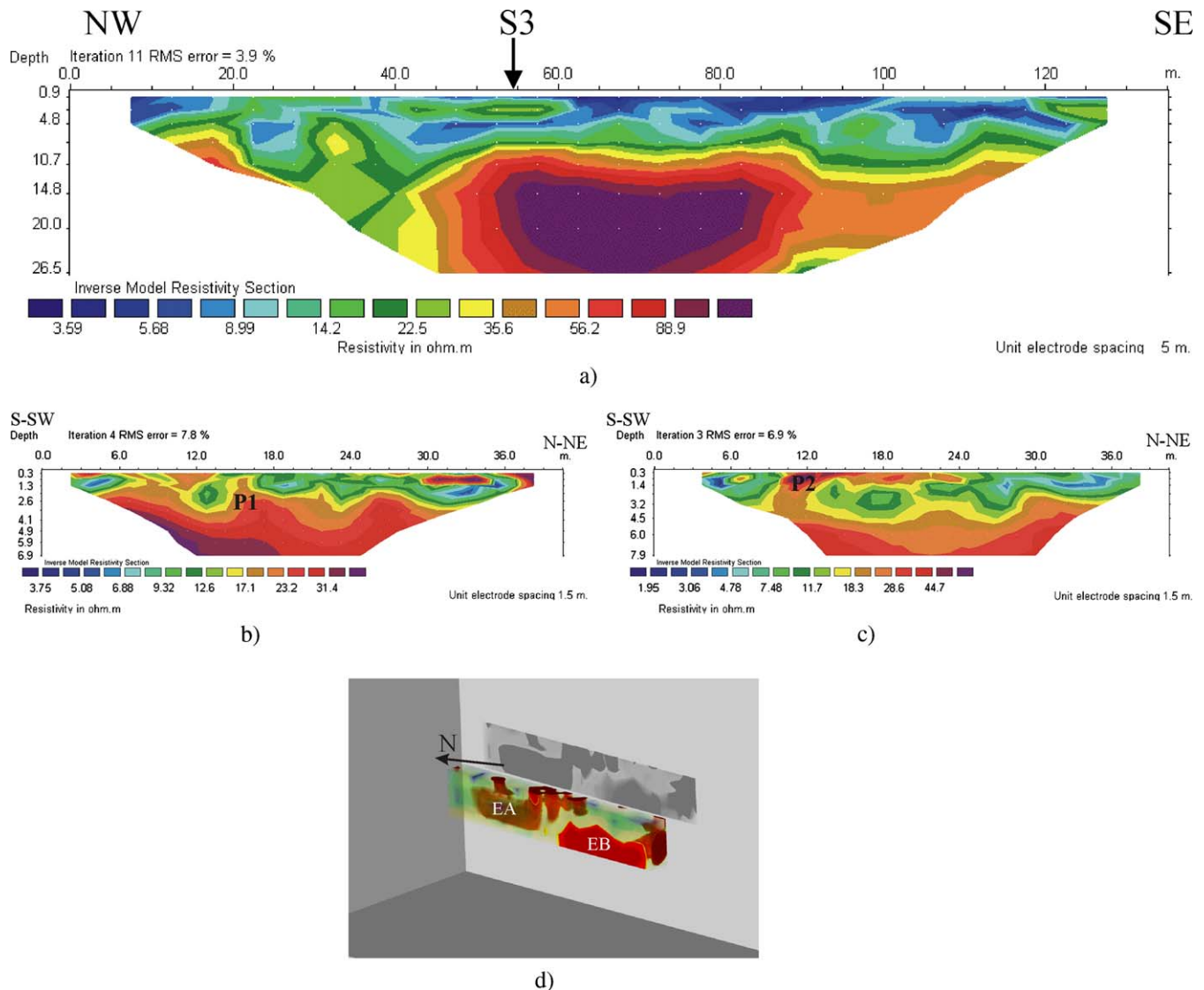


Fig. 8. Electrical tomography sections at the port for lines (a) R1, (b) R2 and (c) R3. (d) Three-dimensional image from electrical tomography survey in Necropolis seen from the southwest (the dimensions of the image are $12 \times 1 \times 1$ m, vertical exaggeration 3:1). Red corresponds to high resistivity.

on the time slice at 2–3 ns (Fig. 9e). The upper anomaly extends further to the NW where it meets another perpendicular linear anomaly. The lower one ends to the SE close to anomaly H1 that is very well delineated on the geophysical maps (Figs. 2 and 4). It is also worth mentioning the improved resolving power of GPR for anomalies H2 and H3. Higher resolution is accomplished on a portion of grid H that was scanned with the 450 MHz antennas (Fig. 9g,h). The depth slice at 0–0.65 m (Fig. 9b), deduced from a 3D electrical tomography experiment, is also displayed for comparative purposes.

7. The seismic refraction survey

A shallow seismic survey was carried out in an effort to locate and map the ancient port. The target layer

(basement) consists of Permian-Triassic phyllites covered by recently deposited sediments. Seismic refraction is especially suited for shallow investigations. Eight profiles have been selected (Fig. 10b) with total length of 580 m and geophone spacing 2 m. The resonance frequency of the geophones was 14 Hz. The hammer and the seisgun (Betsy) produced seismic waves. The Geometrics ES2401 seismograph was used. The detailed description of the seismic experiment is given in Vafidis et al. [24]. Five shots were selected for most seismic lines: one in the middle, two near shots at the edges of the line and two far shots. The third layer (Fig. 10a) shows an increased velocity of 3233 m/s, and is attributed to the basement or to an eroded layer on top of the basement.

Seismic, geological and topographic data were utilized for the creation of a top-to-bedrock image (Fig. 10b). In particular, the elevation of the bedrock

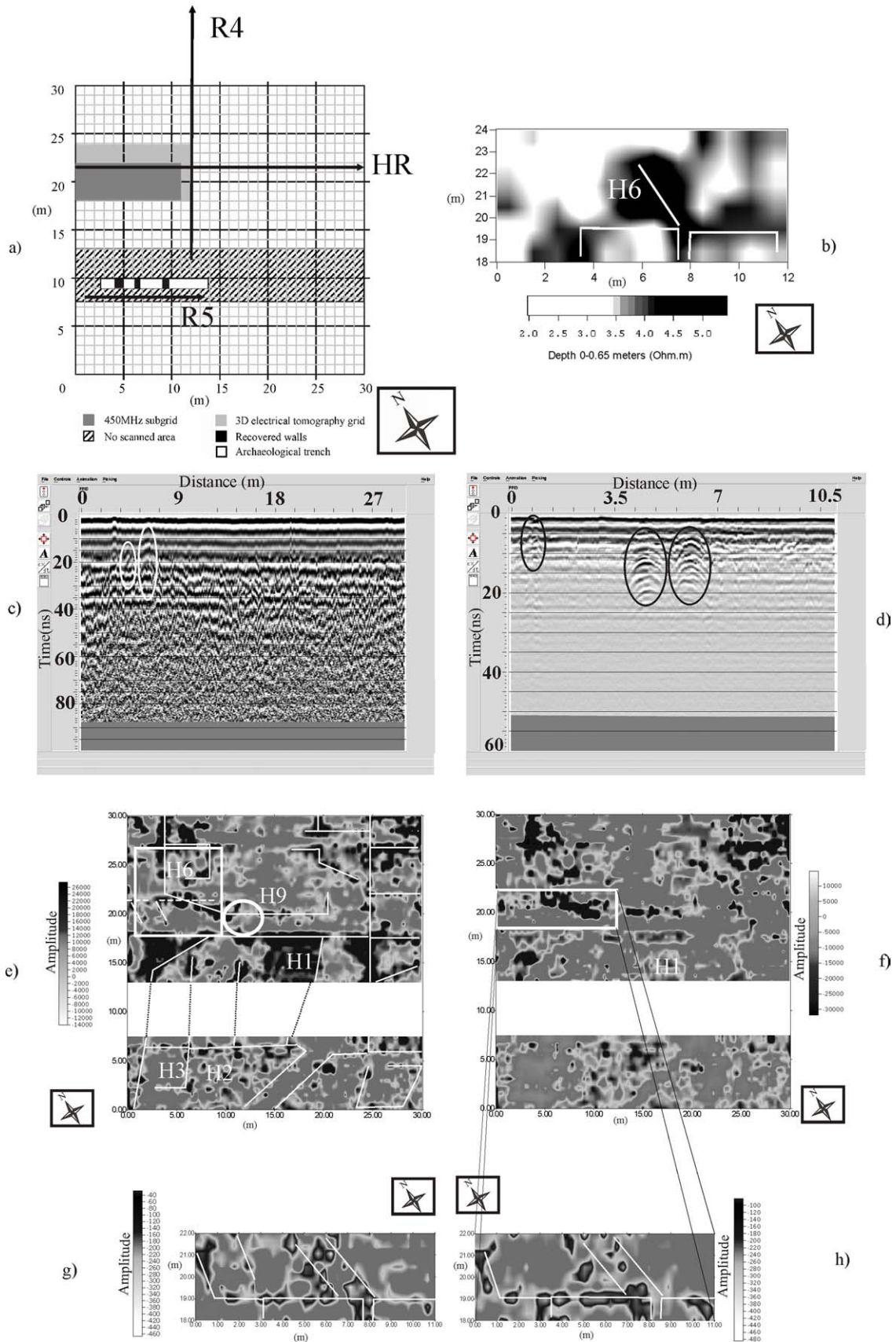


Fig. 9. (a) Details from grid H. Resistivity slice (b) at depth 0–0.65 m from the 3D electrical tomography survey. Ground penetrating radar sections for line HR using the 225 MHz (c) and 450 MHz (d) antennas. Time slices from the GPR survey grid H using the 225 MHz antennas at 2–3 ns (e) and 4–5 ns (f), as well as the 450 MHz antennas at 14–15 ns (g) and 18–19 ns (h). Black corresponds to anomalies probably caused by walls.

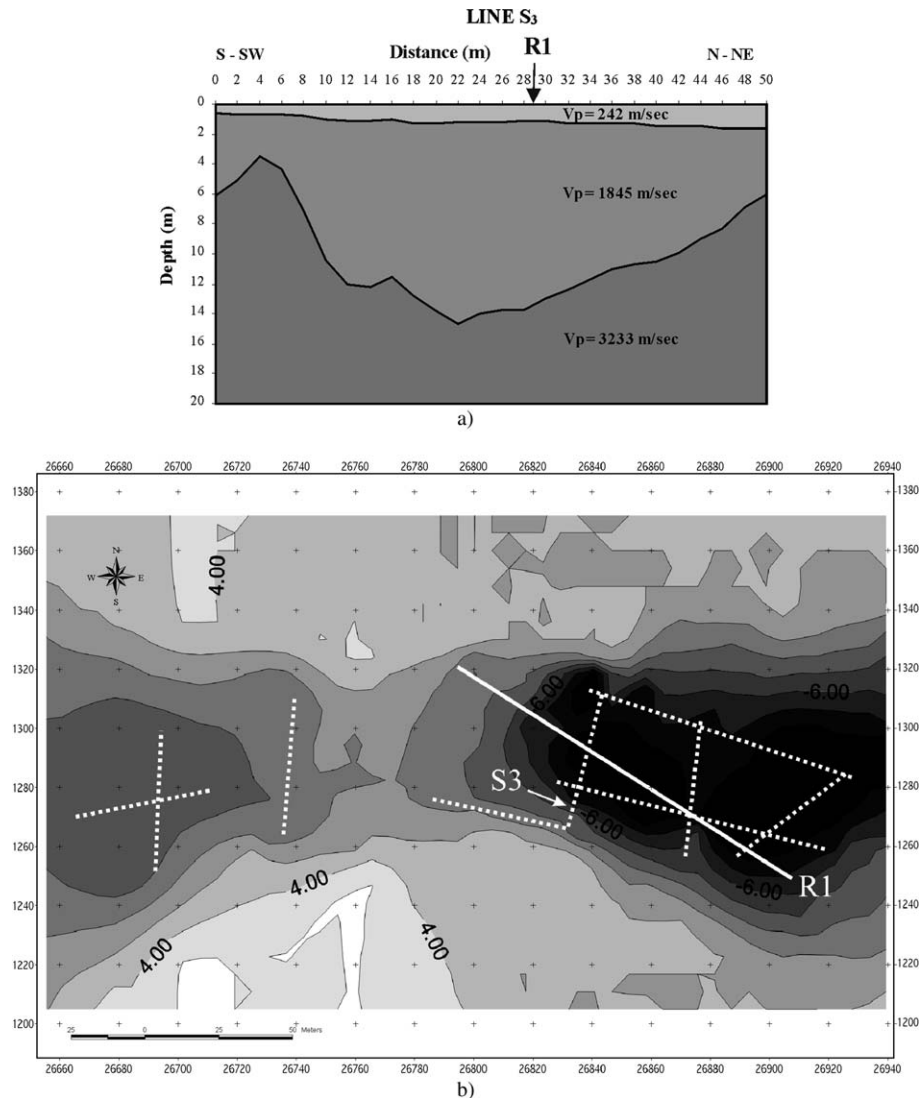


Fig. 10. (a) Depth section from seismic refraction experiment for line S3. (b) Basement relief map (depth to the surface). Black corresponds to low elevation. The spacing of the contours is 2 m. Dotted lines correspond to the seismic lines.

was obtained from the interpolation of the seismic refraction data. It covers a rectangular region of approximately 1500 m², surrounded by the sea, the acropolis to the north and a hill to the south. This image indicates that the ancient port, covered by colluvium, is located south of the acropolis [24]. It extends to the west about 100 m from the present seashore.

The image of the basement relief correlates well with the results from soil resistance mapping, conductivity mapping and electrical tomography. The high resistance anthropogenic anomalies P1, P2, on the soil resistance map (Fig. 7) and electrical tomography depth sections (Fig. 8) are located at places where the basement exhibits depths less than 5–6 m from the surface (or absolute height –3 to –4 m). The three-dimensional image of the basement relief correlates also well with the geoelectric section (Fig. 8a) deduced from the electrical tomography survey along the line R1. The 35 ohm-m

contour of this image exhibits depths (with an accuracy of ± 2.5 m) compatible to those of the top of the basement, deduced from the seismic refraction survey (Fig. 10b). In particular, the seismic velocity model for line S3 (Fig. 10a) and electrical tomography image (Fig. 8a) exhibit depths to the basement 12–14 m (or absolute height –10 to –12 m) at the intersection of lines S3 and R1. A pit is observed to the east on the electrical tomography image (Fig. 8a), at horizontal distance 105 m and on the image of the basement relief at (26880E, 1260N, Fig. 10b).

8. Conclusions

Magnetic gradient, soil resistance and electromagnetic measurements showed several potential targets. In grids M and T, a small portion of the city plan is



Fig. 11. Photograph of the excavated trench on grid H. Arrows indicate wall remains.

imaged. Grid H, apart from the three excavated walls, encounters a wealth of anthropogenic anomalies. The soil resistance gradient map and the high pass filtered magnetic gradient map indicated the anomaly K5 where excavation revealed a well (Fig. 12) and burned soils.

The integration of geophysical mapping and electrical tomography delineated selected anomalies. In particular, anomalies B5 and K1 on the soil resistance map are attributed to a series of high resistance shallow structures. Ground probing radar and electrical tomography sections crossing the three parallel walls on grid H

showed the vertical extent of these features. Time slices resolved better the elongated anomaly H6, present on soil resistance, magnetic gradient and conductivity maps, indicating that it consists of two parallel anomalies.

The seismic and electrical tomography surveys showed similar features supporting the hypothesis that the ancient port extends onshore to the west. The 35-ohm contour on the resistivity image exhibits depths compatible with those of the top of the basement, deduced from the seismic refraction survey.



Fig. 12. Photograph of the well on grid K.

In this integrated survey geomagnetic, resistivity and conductivity mapping techniques proved useful in locating and mapping anthropogenic anomalies at Itanos. The ground penetrating radar and electrical tomography high-resolution techniques delineated many potential targets. These high-resolution geophysical methods are necessary for confirming anomalies on the geophysical maps attributed to buried relics, since they provide better images of the subsurface targets. Therefore, the integrated approach is preferable in particular for geophysical surveys at complex archaeological areas like Itanos.

Acknowledgements

We thank the Department of Mineral Resources Engineering, Technical University of Crete for covering data acquisition cost. We also thank the French School of Archaeology, Athens, for providing access to the archaeological site and Prof. S. Mertikas for providing GPS data.

References

- [1] B. Bevan, The search for graves, *Geophysics* 56 (1991) 1310–1319.
- [2] R. Blakely, *Potential theory in gravity and magnetic applications*, Cambridge University Press, 1996.
- [3] C. Carr, *Handbook on soil resistivity surveying*, Center for American Archaeology Press, Evanston, IL, 1982.
- [4] A.J. Clark, D. Haddon-Reece, An automatic recording system using the Plessey fluxgate magnetometer, *Prospezioni Archeologiche* 7 (1972) 107–114.
- [5] C. Cox, Satellite imagery, aerial photography and wetland archaeology – an interim report on an application of remote sensing to wetland archaeology: the pilot study in Cumbria, England, *World Archaeology* 24 (1992) 249–267.
- [6] L. Conyers, D. Goodman, *Ground-penetrating radar*, AltaMira Press, USA, 1997.
- [7] D.N.M. Donoghue, D.J. Powlesland, C. Pryor, Integration of remotely sensed and ground based geophysical data for archaeological prospecting using a geographic information system, in: A.P. Cracknell, R.A. Vaughan (Eds.), *Proc. of the 18th Annual Conference of the Remote Sensing Society*, University of Dundee, 1992, pp. 197–207.
- [8] E. Greco, Th. Kalpaxis, A. Schnapp, D. Viviers, E. Carando, R. De Bonis, C. D’Ercole, P. Duboeuf, J. Francoise, C. Garcia Martin, G. Grivaud, M. Guy, C. Licoppe, N. Massar, A. Sarris, A. Schnapp-Gourbeillon, D. Theodorescu, C. Tsigonaki, A. Tsingarida, A. Vafidis, P. Vitti, O. Voza, M. Xanthopoulou, *Travaux menes en collaboration avec l’ecole Francaise d’Athenes en 1998*, *Bulletin de Correspondance Hellenique* 123 (1999) 515–530.
- [9] J. Kaczor, J. Weymouth, Magnetic prospecting: preliminary results of the 1980 field season at the Toltee Site, *Southeastern Archaeological Conference* 24 (1981) 118–123.
- [10] Th. Kalpaxis, A. Schnapp, D. Viviers, M. Guy, C. Licoppe, A. Schnapp-Gourbeillon, H. Siard, D. Theodorescu, C. Tsigonaki, A. Vafidis, M. Xanthopoulou, *Rapport sur les travaux menes en collaboration avec l’ecole Francaise d’Athenes en 1994*, *Bulletin de Correspondance Hellenique* 119 (1995) 713–736.
- [11] E.R. Kanasevich, *Time sequence analysis*, University of Alberta Press, Edmonton, Canada, 1971.
- [12] M. Karous, *Goelectrical methods of investigation*, SNTL/ALFA, Prague, 1989.
- [13] E. Le Borgne, Susceptibilite magnetique anormale du sol superficiel, *Annales de Geophysique* 11 (1955) 399–419.
- [14] M.H. Loke, R.D. Barker, Rapid least squares inversion of apparent resistivity pseudosections by a quasi Newton method, *Geophysical Prospecting* 44 (1996) 131–152.
- [15] M. Noel, Multielectrode resistivity tomography for imaging archaeology, in: P. Spoerry (Ed.), *Geoprospection in the Archaeological Landscape*, Oxbow Monographs 18, Oxbow, Oxford, 1992, pp. 89–99.
- [16] M. Pipan, I. Finetti, F. Ferigo, Multi-fold GPR techniques with applications to high-resolution studies: two case histories, *European Journal of Environmental and Engineering Geophysics* 1 (1996) 83–103.
- [17] A. Sarris, *Shallow depth geophysical investigation through the application of magnetic and electric resistance techniques*. PhD thesis, Lincoln, University of Nebraska, 1992.
- [18] A. Sarris, R. Jones, Geophysical prospection of archaeological sites in the Mediterranean region, *Journal of Mediterranean Archaeology* 13 (2000) 3–75.
- [19] A. Sarris, A. Vafidis, S. Mertikas, M. Guy, Th. Kalpaxis, *Remote sensing techniques and computer applications for monuments and site assessment of Itanos (E. Crete)*, Abstracts, *Computer Applications in Archaeology Conference (CAA 98)*, Barcelona, 1970.
- [20] S.V. Spyridakis, *Ptolemaic Itanos and Hellenistic Crete*, Zurich, 1970.
- [21] A. Tabbagh, On the comparison between magnetic and electromagnetic prospecting methods for magnetic features detection, *Archaeometry* 26 (1984) 171–182.
- [22] G.N. Tsokas, C.B. Papazachos, A. Vafidis, M.Z. Loucoyannakis, G. Vargemezis, K. Tzimeas, The detection monumental tombs buried in tumuli by seismic refraction, *Geophysics* 60 (1995) 1735–1742.
- [23] G.N. Tsokas, A. Sarris, M. Pappa, M. Bessios, C. Papazachos, P. Tsourlos, A. Giannopoulos, A large scale magnetic survey in Makrygialos (Pieria), Greece, *Archaeological Prospection* 4 (1997) 123–137.
- [24] A. Vafidis, M. Manakou, G. Kritikakis, D. Voganatsis, A. Sarris, Th. Kalpaxis, Mapping the ancient port at the archaeological site of Itanos (Greece) using shallow seismic methods, *Archaeological Prospection* 10 (2003) 163–173.
- [25] A. Vafidis, A. Sarris, N. Economou, A. Kalpaxis, Geophysical survey in the archaeological site of Itanos, Lasithi Greece, 1st *Balkan Geophysics Society Ext.*, Abstracts, September 23–27, Athens, pp. 54–55.
- [26] A. Vafidis, G.N. Tsokas, M.Z. Loucoyannakis, K. Vasiliadis, C.B. Papazachos, G. Vargemezis, Feasibility study on the use of seismic methods in detecting monumental tombs buried in tumuli, *Archaeological Prospection* 2 (1995) 119–128.
- [27] C.J. Vaughan, Ground penetrating radar surveys used in archaeological investigations, *Geophysics* 51 (1986) 595–604.
- [28] J.W. Weymouth, R. Huggins, *Geophysical surveying of archaeological sites*. In: *Archaeological Geology*, Yale University Press, New Haven, 1985.